Journal of Magnetic Resonance 200 (2009) 167–172

Contents lists available at ScienceDirect

Journal of Magnetic Resonance

journal homepage: www.elsevier.com/locate/jmr

Communication

Generalized biaxial shearing of MQMAS NMR spectra

John D. Gehman [a,*], John L. Provis [b]

[a] School of Chemistry and Bio21 Institute, University of Melbourne, 30 Flemington Rd., Vic. 3010, Australia
[b] Department of Chemical and Biomolecular Engineering, University of Melbourne, Vic. 3010, Australia

ARTICLE INFO

Article history:
Received 29 April 2009
Revised 19 June 2009
Available online 26 June 2009

Keywords:
Multiple quantum magic angle spinning (MQMAS)
Spectral shearing
Amorphous solids
Half-integer NMR nuclei
O-17
Geopolymer

ABSTRACT

Two dimensional multiple quantum (MQ) MAS NMR experiments have become popular due to the wide applicability of this technique to structural questions in materials science, the abundance of half-integer spin nuclei in the periodic table, and the ease of implementation on typical solid state NMR instruments. In spite of the high-resolution theoretically possible from such experiments, the homogeneous and inhomogeneous broadening factors inherent in many samples of interest can make spectral analysis challenging. We present several possible spectral shearing schemes that may be useful for spectral analysis, and in particular we introduce shearing in the directly detected dimension. We suggest that for amorphous or disordered samples that give broad spectral features, shearing may be used as a general tool for optimal positioning of these features relative to one another and for the characterization of isotropic chemical and quadrupolar shifts.

© 2009 Elsevier Inc. All rights reserved.

1. Introduction

Since its introduction in 1995 [1], multiple quantum magic angle spinning (MQMAS) correlation spectroscopy has become popular for high-resolution NMR spectra of half-integer quadrupolar nuclei. While double angle spinning (DAS) and double rotation (DOR) experiments enable similar analysis of materials by averaging both the second and fourth-order Legendre polynomials that modulate the substantial second and fourth rank quadrupolar coupling terms, the MQMAS approach can be performed with typical MAS instrumentation and equipment without specialized hardware. Sample spinning is conducted only at 54.74°, which removes the second rank quadrupolar coupling by averaging the second-order Legendre polynomial to zero at sufficiently fast spin rates. High-resolution in the MQMAS experiment is achieved by partial averaging of the fourth-order Legendre polynomial; the conversion of symmetric multiple quantum coherence (pQ) to the single quantum ($1Q$) central transition for detection; and drawing the pQ and $1Q$ correlations out into two dimensions.

Several conventions for spectral processing of the indirect dimension are in use [2,3] to facilitate the interpretation of MQMAS spectra. While each convention has substantial merit and benefit, the lack of consensus can make the literature confusing. In the interest of simplicity, and because this work does not specifically address this problem of manipulating the indirect dimension, we use similar conventions and terms as Medek [4,5], except as specified. This convention does not scale, shift, or reverse the frequency axes.

Using this convention, the evolution of coherence order p under sufficiently fast MAS conditions (and/or employing rotor synchronized acquisition in the indirect dimension [6]) occurs at frequencies ν_p according to [5,7,8],

$$\nu_p = -p\nu_0^{cs} + C_0^p\nu_0^Q + C_4^p\nu_4^Q(\theta,\phi), \tag{1}$$

for the isotropic chemical shift ν_0^{cs}; isotropic (rank zero) second-order quadrupolar shift

$$\nu_0^Q = -\frac{C_Q^2}{10\nu_L}\frac{1}{[2I(2I-1)]^2}\left(\eta_Q^2+3\right); \tag{2}$$

and rank 4 orientation-dependent frequencies

$$\begin{aligned}\nu_4^Q(\theta,\phi) = \frac{C_Q^2}{1120\nu_L}\frac{7}{18}\frac{1}{[2I(2I-1)]^2}\times\Big\{&9\left(35\sin^4\theta-40\sin^2\theta+8\right)\\&+30\eta_Q\cos 2\phi\left(6\sin^2\theta-7\sin^4\theta\right)\\&+\eta_Q^2\left(35\cos^2 2\phi\sin^4\theta-20\sin^2\theta+4\right)\Big\},\end{aligned} \tag{3}$$

with quadrupolar coupling constant $C_Q = e^2qQ/h$ in Hz, quadrupolar asymmetry η_Q, Larmor frequency ν_L, half-integer spin I, polar angle θ, azimuthal angle ϕ, and a factor of $-7/18$ in ν_4^Q accounts for partial averaging of the fourth-order Legendre polynomial under

* Corresponding author.
E-mail address: jgehman@unimelb.edu.au (J.D. Gehman).

1090-7807/$ - see front matter © 2009 Elsevier Inc. All rights reserved.
doi:10.1016/j.jmr.2009.06.016

MAS. The isotropic and rank 4 Clebsch–Gordan-derived coefficients are

$$C_0^p = p\left[I(I+1) - \frac{3}{4}p^2\right] \tag{4}$$

$$C_4^p = p\left[18I(I+1) - \frac{17}{2}p^2 - 5\right]. \tag{5}$$

Generally, in the pulse sequences used to obtain MQMAS spectra [9], the symmetric pQ coherence (i.e. the $-p/2 \leftrightarrow p/2$ transition) evolves in t_1, and is converted to the central $p = -1$ coherence for direct detection in t_2. These dimensions then transform into indirectly and directly detected frequency axes ν_1 and ν_2, respectively, as usual [10]. Residual second-order quadrupolar coupling anisotropy lineshapes described by the $\nu_4^Q(\theta,\phi)$ term align along ridges with a slope of

$$k = \frac{\Delta\nu_1}{\Delta\nu_2} = \frac{C_4^p}{C_4^{\bar{1}}}, \tag{6}$$

and center of mass defined by the isotropic shielding and quadrupolar shifts.

2. Spectral shearing

Common to MQMAS spectral processing schemes, except the split-t_1 experiment [11], is a shearing transformation in the ν_1 indirect dimension which can be represented by

$$\begin{pmatrix} \nu_1' \\ \nu_2 \end{pmatrix} = \begin{pmatrix} 1 & a \\ 0 & 1 \end{pmatrix}\begin{pmatrix} \nu_1 \\ \nu_2 \end{pmatrix} \tag{7}$$

with ν_2 zero frequency set to the carrier. The shear-transformed dimension becomes

$$\nu_1' = (a-p)\nu_{iso}^{CS} + C_0^{\bar{1}}[a+\lambda]\nu_0^Q + C_4^{\bar{1}}(k+a)\nu_4^Q, \tag{8}$$

with [3]

$$\lambda = \frac{C_0^p}{C_0^{\bar{1}}}. \tag{9}$$

The shearing factor a is to some extent a matter of choice. For the commonly used $a = -k$, the indirect pQ evolution dimension loses the anisotropic second-order quadrupolar term ν_4^Q, and projections onto the ν_1' axis are a function of isotropic shielding and quadrupolar shifts only. Another approach is to shear the indirect dimension instead with $a = p$ [12,13]. The isotropic chemical shift is thus lost from the indirect dimension, which becomes purely a function of the quadrupolar coupling parameters, at the expense of a widening and shearing of the second-order quadrupolar broadening.

The suggestion arises that the choice of shearing factor should be made on a case-by-case basis. Where distinct chemical sites are well resolved, as for many model compounds presented in the literature, shearing by $-k$ appears to be the best choice. Amorphous or disordered materials, on the other hand, typically give a distribution of chemical shift and/or quadrupolar parameters, and it can be more difficult to interpret MQMAS spectra to identify distinct chemical sites. Where the distribution of chemical shifts leads to greater inhomogeneous linewidths than the second-order quadrupolar broadening, eliminating chemical shift in the indirect dimension by shearing with a factor p can lead to apparently sharper spectra and therefore enhanced ability to distinguish dissimilar sites.

Inspection of Eq. (7) together with the equations represented by the frequencies ν_1, ν_2 and ν_1' indicates that shearing simply represents a step of Gauss-Jordan elimination, even while ν_0^Q and ν_4^Q are both functions of C_Q and η_Q and therefore not independent.

We note that additional shearing in the directly detected dimension by an appropriate factor, akin to a second step of Gauss-Jordan elimination, can provide further cosmetic modifications of the spectra which may aid interpretation by helping to identify and characterize independent chemical sites. The full operation relating biaxially sheared spectral frequencies to physical NMR parameters for the $pQ \rightarrow -1Q$ experiment can be represented as:

$$\begin{pmatrix} \nu_1' \\ \nu_2' \end{pmatrix} = \begin{pmatrix} 1 & a \\ b & (1+ab) \end{pmatrix}\begin{pmatrix} -p & C_0^p & C_4^p \\ 1 & C_0^{\bar{1}} & C_4^{\bar{1}} \end{pmatrix}\begin{pmatrix} \nu_0^{cs} \\ \nu_0^Q \\ \nu_4^Q \end{pmatrix} \tag{10}$$

The second shearing can be easily implemented by using the same algorithm as the first shearing operation after transposing the 2D data matrix. Conversely, the two isotropic physical NMR parameters (ν_0^{cs} and ν_0^Q) can be extracted from the frequencies at the center-of-mass along the $\nu_2 = 1Q$ axis by:

$$\begin{pmatrix} \nu_0^{cs} \\ \nu_0^Q \end{pmatrix} = \frac{1}{\left(C_0^p + pC_0^{\bar{1}}\right)}\begin{pmatrix} -C_0^{\bar{1}} & C_0^p \\ 1 & p \end{pmatrix}\begin{pmatrix} (1+ab) & -a \\ -b & 1 \end{pmatrix}\begin{pmatrix} \nu_1' \\ \nu_2' \end{pmatrix} \tag{11}$$

Two of the obvious biaxial shearing factor combinations a, b are $-k, 1/(p+k)$ and $p, -1/(p+\lambda)$. Explicit equations for the transformed frequency axes for both uniaxial shearing $(a, 0)$ and these biaxial shearing combinations, together with the corresponding admixture of these frequencies to give NMR parameters, are given in Table 1.

3. Experimental methods

Samples of amorphous potassium aluminosilicate gel ("geopolymer" [15]) were synthesized by mixing ^{17}O-enriched potassium silicate solution with a powder of composition $2SiO_2 \cdot Al_2O_3$

Table 1
Relationship between spectral (ν_3Q and ν_{1Q}) and NMR parameters (ν_0^{cs}, ν_0^Q and ν_4^Q), in terms of $k = C_4^p/C_4^{\bar{1}}$ (Eq. (6)) and $\lambda = C_0^p/C_0^{\bar{1}}$ (Eq. (9)), after shearing by different factors a, b according to Eq. (10).

$-k, 0$	$\nu_{3Q}' = -(k+p)\nu_0^{cs} + [\lambda - k]C_0^{\bar{1}}\nu_0^Q$ $\nu_{1Q} = \nu_0^{cs} + C_0^{\bar{1}}\nu_0^Q + C_4^{\bar{1}}\nu_4^Q$	$\nu_0^{cs} = -[1/(p+\lambda)]\nu_{3Q}' + [(\lambda-k)/(p+\lambda)]\nu_{1Q}$ $\nu_0^Q = (1/C_0^{\bar{1}})[1/(p+\lambda)]\nu_{3Q}' + (1/C_0^{\bar{1}})[(p+k)/(p+\lambda)]\nu_{1Q}$
$-k, 1/(p+k)$	$\nu_{3Q}' = -(k+p)\nu_0^{cs} + [\lambda - k]C_0^{\bar{1}}\nu_0^Q$ $\nu_{1Q}' = [(p+\lambda)/(p+k)]C_0^{\bar{1}}\nu_0^Q + C_4^{\bar{1}}\nu_4^Q$	$\nu_0^{cs} = [-1/(k+p)]\nu_{3Q}' + [(\lambda-k)/(p+\lambda)]\nu_{1Q}'$ $\nu_0^Q = (1/C_0^{\bar{1}})[(p+k)/(p+\lambda)]\nu_{1Q}'$
$p, 0$	$\nu_{3Q}' = (p+\lambda)C_0^{\bar{1}}\nu_0^Q + (C_4^p + pC_4^{\bar{1}})\nu_4^Q$ $\nu_{1Q} = \nu_0^{cs} + C_0^{\bar{1}}\nu_0^Q + C_4^{\bar{1}}\nu_4^Q$	$\nu_0^{cs} = -[1/(p+\lambda)]\nu_{3Q}' + \nu_{1Q}$ $\nu_0^Q = (1/C_0^{\bar{1}})[1/(p+\lambda)]\nu_{1Q}$
$p, -1/(p+\lambda)$	$\nu_{3Q}' = (p+\lambda)C_0^{\bar{1}}\nu_0^Q + (C_4^p + pC_4^{\bar{1}})\nu_4^Q$ $\nu_{1Q}' = \nu_0^{cs} + [(-C_4^p + \lambda C_4^{\bar{1}})/(p+\lambda)]\nu_4^Q$	$\nu_0^{cs} = \nu_{1Q}'$ $\nu_0^Q = (1/C_0^{\bar{1}})[1/(p+\lambda)]\nu_{3Q}'$

prepared by the PVA method of Gülgün et al. [16]. Enriched potassium silicate solutions were prepared by combining 10% ^{17}O-enriched water (Cambridge Isotopes) with KOH pellets (Aldrich) and silica fume (Aerosil 200, Degussa), and were allowed to sit for 24 h to allow equilibration of the dissolved silicate species before use in geopolymer synthesis. Samples were formulated to have overall compositions $K_2O \cdot nSiO_2 \cdot Al_2O_3 \cdot 11H_2O$ with $n = 2.5$ and 3.5; i.e. nominal Si/Al ratios of 1.25 and 1.75. The actual Si/Al ratios of the aluminosilicate gels formed via attack of the ^{17}O-enriched silicate solution on the unenriched solid precursor particles (and which therefore contain all of the ^{17}O observable) are somewhat lower than the nominal values due to the presence of an unreactive (although X-ray amorphous) silicate phase in the powder precursor. The sample at nominal Si/Al = 1.25 showed an apparent gel Si/Al ratio close to 1.0 as determined by the appearance of a single peak (Si–^{17}O–Al) in its ^{17}O MQMAS NMR spectrum, and the presence of a sharp peak in ^{29}Si MAS NMR spectra of hardened samples assigned to an ordered and unreactive silicate phase in the remnant solid precursor (data not shown). Overall ^{17}O enrichment in the aluminosilicate gel formed was around 3%. Samples were cured at 40 °C for 24 h then at ambient temperature for 2 weeks, and dried at ~100 °C to remove free water prior to analysis.

Solid-state NMR spectroscopy was performed at 19.6 T (^{17}O frequency of 112.437 MHz) at the National High Magnetic Field Laboratory (Tallahassee, FL), using a Bruker DRX spectrometer, a 4-mm MAS probe and a shifted whole-echo 3QMAS experiment with 1 ms fixed delay between the $3Q \rightarrow 1Q$ conversion and the selective echo pulses. Spectra were collected with 50 and 10 kHz spectral widths in the direct and indirect dimensions, respectively, 24 t_1 increments, and an MAS spin rate of 10 kHz. The experimental data were not apodized. All data were processed with NMRPipe [17].

Table 2
Physical NMR parameters used for the different sites in simulations (Fig. 1).

	ν_0^{cs}/ν_0 (ppm)	C_Q (MHz)
A	0	1.25
B	0	3.0
C	0	5.0
D	−20	5.0
E	30	5.0

Simulations were performed with Simpson [18], using the same experimental parameters as those used in experiments described above, and processed identically also with NMRPipe, except for the apodization with Gaussian line-broadening of 120 and 220 Hz in the direct and indirect dimensions, respectively, to mimic the finite signal lifetime. Fig. 1 shows ^{17}O 3QMAS shifted-echo spectra of five hypothetical sites. To more clearly illustrate the slopes along which the NMR parameters vary under the different shearing schemes, three of the simulated sites were given the same isotropic chemical shift with negligible CSA but with varying quadrupolar couplings, and three were given varying isotropic chemical shifts with identical quadrupolar parameters (Table 2). The simulated spectra of Fig. 1 also serve to represent spectra with well resolved sites and narrow linewidths in the pQ dimension, similar to an ideal "crystalline" site.

4. Spectral analysis

Inhomogeneous and homogeneous broadening of $pQ - 1Q$ signal correlations can make it difficult to identify and characterize different chemical sites within a spectrum. Characterization of chemical inhomogeneity can itself be of particular interest in the

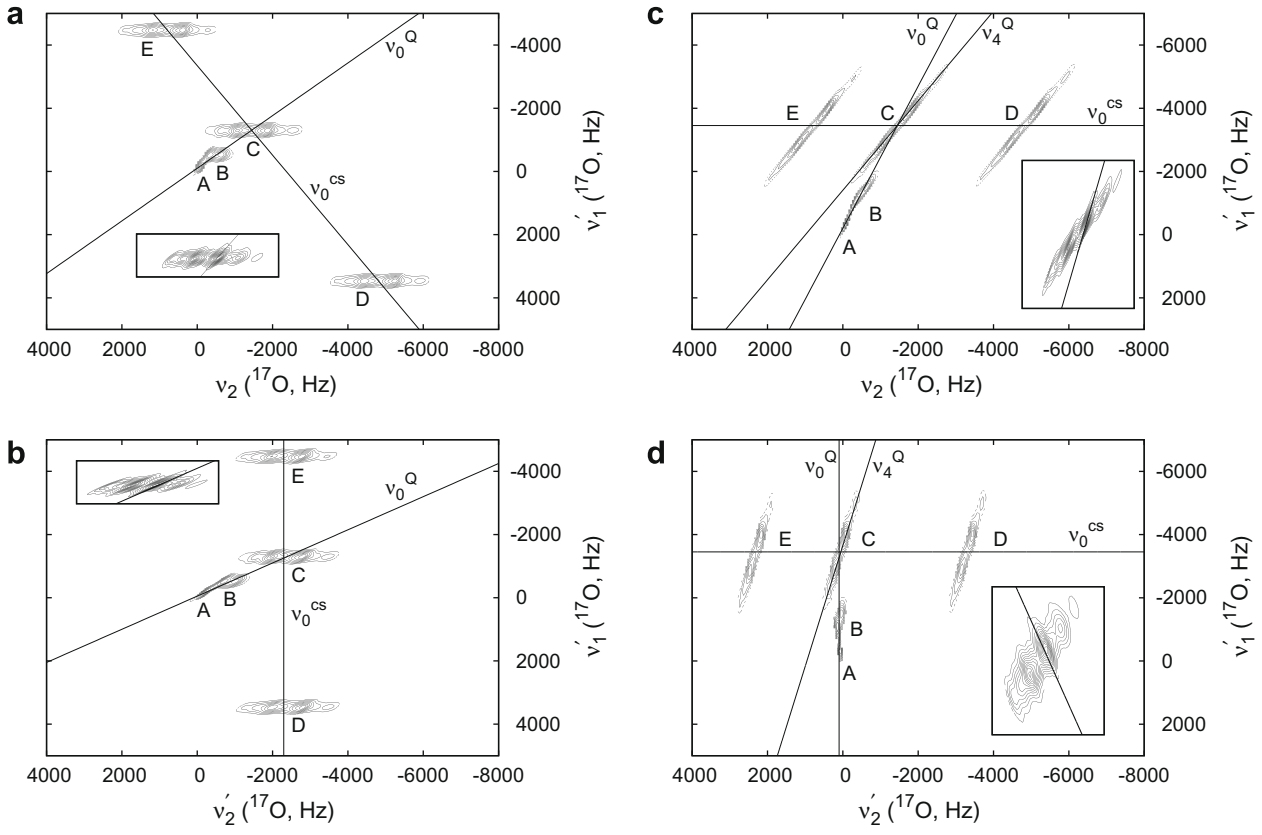

Fig. 1. ^{17}O 3QMAS NMR spectra of simulated sites using $\eta_Q = 0.5$ and different chemical shift $\delta = \nu_0^{iso}/\nu_0$ and C_Q values as given in Table 2. Spectra are sheared in the ν_{3Q}, ν_{1Q} axis, respectively, by: (a) 19/12, 0; (b) 19/12, 12/17; (c) 3,0; and (d) 3, −4/9. Slopes given in Table 3 are shown, except for the zero slopes for ν_4^Q in (a) and (b). Inset: Gaussian apodization is increased on one chemical site to simulate homogeneous broadening. Lines through this peak have the slopes given for $\Delta\nu^{homo}$ in Table 3.

Table 3
Slopes of NMR parameter axes (including homogeneous broadening) after shearing in the ν_{3Q}, ν_{1Q} dimension with factors a, b, respectively, for spin $I = 5/2$. Note that isotropic shifts for 19/12, 0 agree with Bodart [14] and Millot and Man [3] for an unreversed directly detected frequency axis.

	0, 0	19/12, 0	19/12, 12/17	3, 0	3, −4/9
ν_0^{cs}	−3	−17/12	1/0	0	0
ν_0^{Q}	−3/4	5/6	85/162	9/4	1/0
ν_4^{Q}	−19/12	0	0	17/12	153/40
$\Delta\nu^{homo}$	∼ 12/19	∼ 2.21	∼ 0.86	∼ 3.63	∼ 5.91

analysis [19], and may include distributions of chemical shift, quadrupolar parameters, or both. Homogenous broadening, on the other hand, may arise from a variety of mechanisms, such as proximity of large quadrupolar ions.

Chemical shift (ν_0^{cs}), isotropic quadrupolar shift (ν_0^{Q}), and quadrupolar anisotropy of rank 4 (ν_4^{Q}) all transform independently under the shear transformation. A fourth characteristic, the homogeneous broadening ($\Delta\nu^{homo}$) may also be regarded as an independently transforming quantity as shown by Brown and Wimperis; where the extent of broadening is similar during the pQ and $1Q$ evolution periods, the direction of homogeneous broadening may be taken as perpendicular to the unsheared "ridges" along ν_4^{Q}, with slope $\sim -1/k$ [11]. Rigorous treatment of homogenous broadening for different coherences is reported [20], and may provide important corrections to this generalization where high-resolution spectra are obtained. The slopes of the axes over which these four physical NMR parameters vary within the frequency axis systems are given for a spin $I = 5/2$ nucleus under the featured shearing factor combinations in Table 3. Observation of the changes in peak shape through these (and other) shearing schemes, with reference to the calculated axis slopes for the physical parameters, can significantly aid data interpretation.

4.1. Simulated data

It can be seen in Fig. 1a that the full anisotropic lineshape is refocused to an isotropic projection onto the ν_1 axis, and the projection onto ν_2' axis is similar to that which would be observed in one-dimensional MAS spectra, thus yielding what are commonly referred to as the "isotropic" and "MAS" axes, respectively. Although the pure isotropic shielding and quadrupolar shift axes run skew to the frequency axes, this presents no problem where projections of the spectral features onto the $3Q$ axes have relatively high-resolution. It may nevertheless be preferable, if isotropic linewidths are narrow enough, to shear along the $1Q$ axis as well (Fig. 1b) so that at least one of the NMR parameters, the isotropic chemical shift, varies only along one of the orthogonal frequency axes. For well resolved sites, there is no real benefit to shearing by any other factor. Fig. 1c and d make it clear, however, that when the anisotropic lineshape is sheared significantly away from a slope of zero, the center-of-mass along the ν_2 axis of each site runs parallel to the calculated slope for ν_4^{Q}.

4.2. Experimental data

Fig. 2 explores the same shear factor combinations as were used for the simulated data, but for a less well defined peak, obtained from the geopolymer sample with Si/Al = 1.25 and attributed to Si–^{17}O–Al bonding. Shearing of the $\nu_2 = 1Q$ axis from Fig. 2a to b again swings the chemical shift axis to the vertical, making the ν_2' axis a "pure quadrupolar" axis. In both Fig. 2a and b, the center-of-mass of the peak along the $\nu_2 = 1Q$ axis runs parallel to

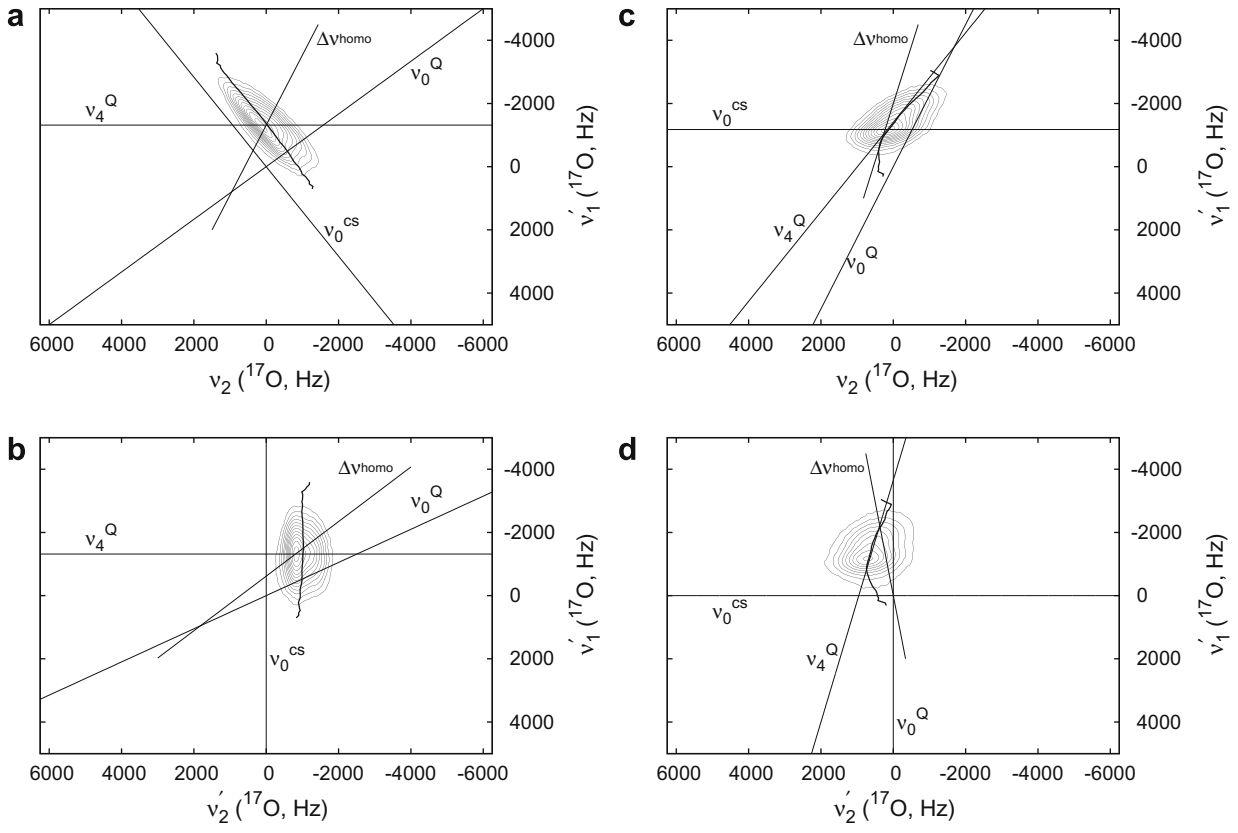

Fig. 2. ^{17}O 3QMAS NMR spectra of geopolymer with Si/Al = 1.25. Spectra are sheared in the ν_{3Q} and ν_{1Q} axes, respectively, by: (a) 19/12, 0; (b) 19/12, 12/17; (c) 3,0; and (d) 3, −4/9. Slopes given in Table 3 are shown. Calculated centre-of-mass along the $1Q$ axis through the spectral feature is also shown as a bold line segment. Lines with slopes given in Table 3 are indicated.

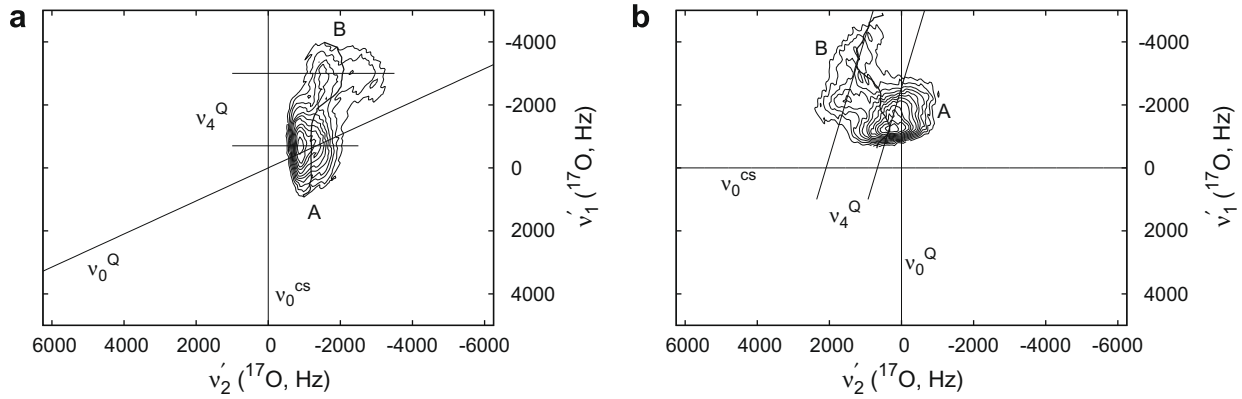

Fig. 3. ^{17}O 3QMAS NMR spectra of geopolymer with Si/Al = 1.75. Spectra are sheared in the ν_{3Q} and ν_{1Q} axes, respectively, by (a) 19/12, 12/17 and (b) 3, −4/9. Slopes given in Table 3 are shown. Calculated centre-of-mass along the 1Q axis through the spectral features is also shown as a bold line segment.

the chemical shift axis, and one would conclude that there is just one chemical site that is distributed with respect to chemical shift.

Assessing lineshape with respect to quadrupolar parameters C_Q and η is more complicated, as each affects both ν_0^Q and ν_4^Q. Slices through the maximum of the peak parallel to the $\nu_2^{(\prime)}$ axis in Fig. 2a and b suggest that $\eta <\sim 0.3$, but with indistinct features owing to broadening. Significantly, the center-of-mass line through the peak does not deviate appreciably in a direction parallel to the ν_0^Q axis. It may therefore be concluded that the broadening of the anisotropic lineshape features along ν_4^Q is primarily homogeneous. Alternatively, the broadening is inhomogeneous, but does not deviate systematically with chemical shift.

Examination of peak contours under different shearing schemes helps to interpret the nature of the broadening. Shearing the $\nu_1 = 3Q$ axis by a factor of $a = p = 3$ results in the "pure quadrupolar" ν_1' axis. A subsequent shearing along the $\nu_2 = 1Q$ axis (Fig. 2d) makes the isotropic quadrupolar-induced and chemical shift axes orthogonal, and aligned parallel to the frequency axes ν_2' and ν_1', respectively. The center-of-mass calculated along $\nu_2^{(\prime)}$ axis again runs parallel to the calculated slope for ν_4^Q, as for the simulated chemical sites in Fig. 1c and d. Through all shearing schemes, there appears to be no tendency of the peak to be broadened along the calculated slopes corresponding to $\Delta\nu^{homo}$; all isotropic linewidths appear to transform as real combinations of chemical shift and quadrupolar isotropic frequencies. Consequently, the finite linewidth which appears convoluted with the anisotropic lineshape is most likely dominated by inhomogeneous broadening by a distribution of quadrupolar parameters. This conclusion is consistent with that expected by having used the shifted-echo pulse sequence, through which homogenous broadening would not refocus.

The shearing scheme used in Fig. 2d might seem like a particularly attractive option for disordered sample MQMAS spectra. It should not, however, be considered a fixed recipe. Fig. 3 shows biaxially-sheared spectra for the sample with Si/Al = 1.75. The more intense Si–^{17}O–Al site appears again, although perhaps with less inhomogeneous broadening by quadrupolar parameters. In this case, however, the center-of-mass clearly diverges to a second segment that also runs parallel to the ν_0^{cs} axis, making the appearance of a second site (Si–^{17}O–Si) obvious. Alternatively, a shearing scheme identical to that in Fig. 2d places the two sites approximately side-by-side along the ν_2' axis (Fig. 3b). This makes the center-of-mass analysis difficult to apply and interpret. In this case, the shearing scheme used in Fig. 2b makes it easy to see that there are two sites, where the center-of-mass along the ν_2' axis runs parallel to the ν_1' axis while traversing each site. Nevertheless, the varying perspectives on broadening provided by different shearing schemes is still valuable.

5. Conclusions

We have demonstrated four possible schemes which may be valuable for shearing MQMAS NMR spectra. The shearing factors used for the indirect dimension were chosen based upon common practice, and shearing factors chosen for the direct dimension (where non-zero) are those which provide for a tidy alignment of physical NMR parameter axes with spectral frequency axes. The possibilities are not limited to these shearing factor combinations; for any combination of shearing factors, a system of equations as in Table 1 can be easily written using Eqs. (10) and (11), and the axes corresponding to the slopes along which NMR parameters vary can be drawn and compared to the center-of-mass line. In practice, several combinations of shearing factors should be explored for spectra displaying broad lines, to lend confidence to the final interpretation and peak assignments. The general principle presented here may also readily be adapted and applied in the various referencing and scaling conventions used in practice for representation of MQMAS NMR data.

Acknowledgment

We wish to thank Zhehong Gan for experiments performed at NHMFL and for enlightening discussion; Claire White and Peter Duxson for their contributions in sample synthesis, technique development and discussion of the ^{17}O MQMAS NMR spectra of aluminosilicate geopolymers; and Professors Frances Separovic and Jannie van Deventer for their support of J.D.G. and J.L.P., respectively. J.D.G. acknowledges support from the University of Melbourne Early Career Research grants scheme. The spectrometer used in this study was funded in part by the Engineering and Physical Sciences Research Council and the National High Magnetic Field Laboratory. Travel funding was supplied by the Access to Major Research Facilities Program administered by the Australian Nuclear Science and Technology Organisation (ANSTO). This work has also received partial financial support from the Australian Research Council (ARC), including via the Particulate Fluids Processing Centre, a Special Research Centre of the ARC.

References

[1] L. Frydman, J.S. Harwood, Isotropic spectra of half-integer quadrupolar spins from bidimensional magic-angle spinning NMR, J. Am. Chem. Soc. 117 (1995) 5367–5368.
[2] J.-P. Amoureux, C. Huguenard, F. Engelke, F. Taulelle, Unified representation of MQMAS and STMAS NMR of half-integer quadrupolar nuclei, Chem. Phys. Lett. 356 (2002) 497–504.

[3] Y. Millot, P.P. Man, Procedures for labelling the high-resolution axis of two-dimensional MQ-MAS NMR spectra of half-integer quadrupole spins, Solid State Nucl. Magn. Reson. 21 (2002) 21–43.
[4] A. Medek, J.S. Harwood, L. Frydman, Multiple-quantum magic-angle spinning NMR: a new method for the study of quadrupolar nuclei in solids, J. Am. Chem. Soc. 117 (1995) 12779–12787.
[5] A. Medek, L. Frydman, Multiple-quantum magic-angle spinning NMR: a new technique for probing quadrupolar nuclei in solids, J. Braz. Chem. Soc. 10 (4) (1999) 263–277.
[6] D. Massiot, Sensitivity and lineshape improvements of MQ-MAS by rotor-synchronized data acquisition, J. Magn. Reson. A 122 (1996) 240–244.
[7] J.-P. Amoureux, High-resolution solid-state NMR for spin 3/2 and 9/2: the multi-quantum transitions method, Solid State Nucl. Magn. Reson. 2 (1993) 83–88.
[8] A. Jerschow, From nuclear structure to the quadrupolar NMR interaction and high resolution spectroscopy, Prog. Nucl. Magn. Reson. Spectrosc. 46 (2005) 63–78.
[9] D. Massiot, B. Touzo, D. Trumeau, J.P. Coutures, J. Virlet, P. Florian, P.J. Grandinetti, Two-dimensional magic-angle spinning isotropic reconstruction sequences for quadrupolar nuclei, Solid State Nucl. Magn. Reson. 6 (1996) 73–83.
[10] J. Jeneer, Ampére International Summer School, Basko Polje, Yugoslavia, 1971.
[11] S.P. Brown, S. Wimperis, Two-dimensional multiple-quantum MAS NMR of quadrupolar nuclei: a comparison of methods, J. Magn. Reson. 128 (1997) 42–61.
[12] J.-B. d'Espinose de Lacaillerie, F. Barberon, K.V. Romanenko, O.B. Lapina, L.L. Polls, R. Gautier, Z. Gan, ^{95}Mo magic angle spinning NMR at high field: improved measurements and structural analysis of the quadrupole interaction in monomolybdates and isopolymolybdates, J. Phys. Chem. B 109 (29) (2005) 14033–14042.
[13] R.L. Vold, G.L. Hoatson, M. Vijayakumar, Variable temperature ^{93}Nb NMR investigation of local structure and polar nanoclusters in lead magnesium niobate/lead scandium niobate solid solutions, Phys. Rev. B 75 (2007) 134105.
[14] P.R. Bodart, Distributions of the quadrupolar and isotropic chemical shift interactions in two-dimensional multiple-quantum MAS NMR spectra, J. Magn. Reson. 133 (1998) 207–209.
[15] P. Duxson, A. Fernández-Jiménez, J. Provis, G. Lukey, A. Palomo, J. van Deventer, Geopolymer technology: the current state of the art, J. Mater. Sci. 42 (9) (2007) 2917–2933.
[16] M.A. Gülgün, M.H. Nguyen, W.M. Kriven, Polymerized organic–inorganic synthesis of mixed oxides, J. Am. Ceramic Soc. 82 (3) (1999) 556–560.
[17] F. Delaglio, S. Grzesiek, G.W. Vuister, G. Zhu, J. Pfeifer, A. Bax, NMRPipe: a multidimensional spectral processing system based on UNIX pipes, J. Biomol. NMR 6 (1995) 277–293.
[18] M. Bak, J.T. Rasmussen, N.C. Nielsen, SIMPSON: a general simulation program for solid-state NMR spectroscopy, J. Magn. Reson. 147 (2) (2000) 296–330.
[19] J.-B. d'Espinose de Lacaillerie, C. Fretigny, D. Massiot, MAS NMR spectra of quadrupolar nuclei in disordered solids: the Czjzek model, J. Magn. Reson. 192 (9) (2008) 244–251.
[20] J.-P. Amoureux, J. Trébosc, Homogenous broadenings in 2D solid-state NMR of half-integer quadrupolar nuclei, J. Magn. Reson. 179 (2006) 311–316.